Three-body fragmentation dynamics of the propene trication produced by 1-MeV/u C^{4+} impact

Zhencen He,[1,2] Mingliang Duan,[1] Zhuohang He,[1] Shuyu Zhang,[2,*] and Zhimin Hu[1,†]

[1]*Key Laboratory of Radiation Physics and Technology of Ministry of Education, Institute of Nuclear Science and Technology, Sichuan University, Chengdu, Sichuan 610064, China*

[2]*West China School of Basic Medical Sciences and Forensic Medicine, Sichuan University, Chengdu, Sichuan 610041, China*

(Received 9 July 2025; accepted 13 April 2026; published 30 April 2026)

The three-body fragmentation dynamics of propene trications [$(H_3C–CH=CH_2)^{3+}$] induced by 1-MeV/u C^{4+} ion impact is investigated using cold-target recoil-ion momentum spectroscopy. Complete kinematical information is obtained for four three-body fragmentation channels: $H^+ + CH_2^+ + C_2H_3^+$, $H^+ + CH_3^+ + C_2H_2^+$, and the channels involving H_2^+ production, i.e., $H^+ + H_2^+ + C_3H_3^+$ and $H_2^+ + CH_2^+ + C_2H_2^+$. By analyzing the fragment momentum correlations visualized in Dalitz plots, Newton diagrams, and native frames, each channel exhibits two distinct sequential processes, with a concerted process uniquely identified in the $H_2^+ + CH_2^+ + C_2H_2^+$ channel. Relative contributions of competing fragmentation pathways are determined. The sequential pathways with CH breakage prior to CC breakage predominate in the channels $H^+ + CH_2^+ + C_2H_3^+$ and $H^+ + CH_3^+ + C_2H_2^+$. Due to comparable timescales, the H_2 formation kinetically competes with the molecular fragmentation. This competition enables fragmentation pathways featuring initial H_2^+ emission, which contribute to two H_2^+ production channels. This study provides valuable insights into understanding the dissociation behaviors of asymmetric hydrocarbon chains under several-MeV/u ion impact, revealing the role of H_2 formation kinetics in molecular fragmentation dynamics.

DOI: 10.1103/6bn6-jgbj

I. INTRODUCTION

The fragmentation dynamics of polyatomic molecules upon collisions with highly charged ions has been a focal point in atomic and molecular physics, offering critical insights into bond-breaking mechanisms, charge redistribution, and energy transfer processes [1,2]. These studies not only are fundamental to understanding the behavior of molecules under extreme conditions, but also have broad implications for applications in radiation biology [3,4], interstellar chemistry [5,6], and plasma physics [7,8]. When multiply charged molecular ions undergo Coulomb explosion, the resulting fragment momentum correlations provide critical insights into dissociation mechanisms (e.g., concerted versus sequential bond breaking) [9–13] as well as underlying processes like proton migration and molecular isomerization [14–18]. Among various techniques, the cold-target recoil-ion momentum spectroscopy (COLTRIMS) [19], with its capability for full-dimensional analysis of fragment momenta, has emerged as a powerful tool for revealing fragmentation mechanisms and reconstructing dynamic correlations.

Organic hydrocarbon molecules are ubiquitous in the universe and play crucial roles in planetary atmospheres and industrial applications. Significant progress has been made in characterizing the complex fragmentation behaviors of hydrocarbons when exposed to different ionization fields, e.g., CH_4 [20–23], C_2H_2 [24–32], C_2H_4 [33–35], C_3H_4 isomers [36–44], and C_6H_6 [45–48]. Previous studies revealed a rich variety of fragmentation processes, including concerted and sequential cleavages of carbon-carbon (CC) and carbon-hydrogen (CH) bonds, isomer effects [39–42], hydrogen migration [16,18,35,43], etc. For instance, both concerted and sequential processes were involved in the three-body fragmentation of hydrocarbons [32,35,42], with the specific pathways depending on factors such as the projectile velocity and the molecular geometry. Comparative studies with isomers, like propyne and allene, suggested that the structural isomerism significantly influenced fragmentation patterns [39–43].

Propene ($H_3C–CH=CH_2$), as one isomer of C_3H_6 [49], features the coexistence of its unique CC double-bond structure and a methyl (CH_3) group, making it a prototype to study competitive bond-breaking characteristics in its fragmentation dynamics. However, only a few works have reported the fragmentation processes of C_3H_6 isomers [50–52]. A combined experimental and theoretical study of dissociative double photoionization of cyclopropane revealed how specific photon energies selectively trigger ring-opening or ring-closing deformations in the cyclopropane dications [$(H_2C–CH_2–CH_2)^{2+}$] via Jahn-Teller effects [50]. Under 4-keV/u Ar^{8+} impact, the distinct isomer-dependent fragmentation dynamics of propene and cyclopropane ($C_3H_6^{2+}$ dications) were investigated [51]. Most recently, sequential fragmentation mechanisms were revealed to dominate the three-body dissociation of cyclopropane trications [$(H_2C–CH_2–CH_2)^{3+}$] induced by 5.8-MeV/u Ni^{19+} ions, and distinct pathways were identified based on the bond-breaking order of CH and CC bonds [52]. Compared with the ring-structure cyclopropane, the chain structure of propene enables

*Contact author: zhang.shuyu@hotmail.com
†Contact author: huzhimin@scu.edu.cn

the CC double bond to participate in fragmentation processes, just like ethylene [35] and allene [43], potentially triggering unique dissociation phenomena such as the displacement of hydrogen atoms, CC double-bond cleavage, and structural rearrangement. Nevertheless, studies on propene remain scarce, particularly for its triply charged states. In the following, the C_3H_6 molecule is referred to as propene unless specified otherwise.

In this work we investigate the three-body fragmentation of $C_3H_6^{3+}$ induced by 1-MeV/u C^{4+} impact. Utilizing the COLTRIMS technique, the momentum vectors of all fragment ions are measured. Four completely measured fragmentation channels are identified definitely, i.e., (I) $C_3H_6^{3+} \rightarrow H^+ + CH_2^+ + C_2H_3^+$, (II) $C_3H_6^{3+} \rightarrow H^+ + CH_3^+ + C_2H_2^+$, and two channels involving H_2^+ generation, (III) $C_3H_6^{3+} \rightarrow H^+ + H_2^+ + C_3H_3^+$ and (IV) $C_3H_6^{3+} \rightarrow H_2^+ + CH_2^+ + C_2H_2^+$. With the aid of the Dalitz plot, Newton diagram, and native frame method, the momentum correlations between three fragments are displayed, and the fragmentation mechanisms of each dissociation channel are identified and discussed in detail.

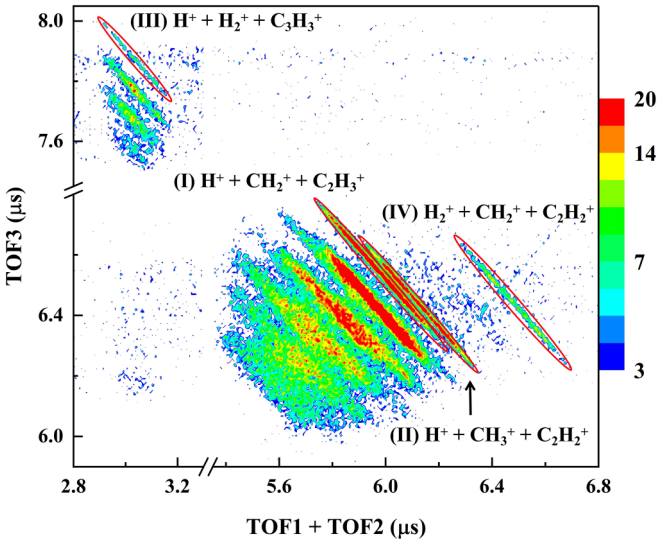

FIG. 1. Triple-ion coincidence TOF map of the collisions of C_3H_6 with 1-MeV/u C^{4+}.

II. EXPERIMENTS AND DATA ANALYSIS

The present experiment was carried out using a COLTRIMS setup mounted on the 3-MV Tandetron accelerator at Sichuan University. Details of the COLTRIMS can be found elsewhere [53,54], so here only a brief description will be given. A 1-MeV/u C^{4+} ion beam perpendicularly crossed a cold supersonic jet produced by the pure propene gas with a pressure of 1 bar passing through a 20-μm nozzle into the high-vacuum collision chamber. Following ion-molecule interaction, recoil ions from molecular ionization and dissociation were extracted and accelerated by a 60-V/cm uniform electrostatic field, traveled through a field-free drift tube, and finally were detected by a position-sensitive detector (PSD) equipped with two multichannel plates (MCPs) and a delay-line anode. The front surface of MCPs was biased 1900 V, negative relative to the ground in the present experiment. Simultaneously, the electrons created in the collisions were extracted in opposite directions to the recoil ions and detected by another PSD. In the coincidence measurement, the time of flight (TOF) of the recoil ion was determined by taking the arriving time of the electron as a reference and recorded by the multihit time-to-digital converter. The three-dimensional momenta of all recoil ions were reconstructed from the hitting TOF and position information.

The TOF information was used to identify ion species, and different fragmentation channels were distinguished from the coincidence TOF map. To reveal the molecular dissociation mechanism, the Dalitz plot and Newton diagram were utilized to visualize the momentum vector relations [2]. In a Dalitz plot, the experimental events are placed inside a circle inscribed in an equilateral triangle. The coordinates X and Y corresponding to each event are given by

$$X = \frac{p_1^2 - p_2^2}{\sqrt{3}\sum p_i^2}, \tag{1}$$

$$Y = \frac{p_3^2}{\sum p_i^2} - \frac{1}{3}, \tag{2}$$

where p_i ($i = 1$, 2, and 3) is the momentum of the ith fragment. In a Newton diagram, the momentum of the first fragment is set at one arbitrary unit and represented by an arrow along the horizontal axis, while the momenta of the second and third fragments are normalized to that of the first fragment and placed in the lower and upper halves of the diagram, respectively. For the representations of sequential processes via Newton diagrams, the centers of the semicircles where the two fragments produced in the second fragmentation step are located are precisely determined by the mass ratio.

The native frame method allows for providing detailed information on each step of the sequential fragmentation and demonstrates that the signature of sequential dissociation is a uniform distribution [11,55]. In the native frames, all fragmentation processes are assumed to be sequential with a metastable intermediate and plotted as a function of $\cos\theta$ and the kinetic energy release (KER) of the intermediate in the second step. Here θ is defined as the angle between the fragmentation axis of the parent ion of the first step and the fragmentation axis of the intermediate ion of the second step in the center-of-mass frame. The $\cos\theta$ distribution is isotropic for rotation on a sphere [55] and is given by

$$\cos\theta = \frac{\Delta\mathbf{P}_{1\mathrm{st}} \cdot \Delta\mathbf{P}_{2\mathrm{nd}}}{|\Delta\mathbf{P}_{1\mathrm{st}}||\Delta\mathbf{P}_{2\mathrm{nd}}|}. \tag{3}$$

Here $\Delta\mathbf{P}_{1\mathrm{st}} = [(m_2 + m_3)\mathbf{p}_1 - m_1(\mathbf{p}_2 + \mathbf{p}_3)]/(m_1 + m_2 + m_3)$ and $\Delta\mathbf{P}_{2\mathrm{nd}} = (m_3\mathbf{p}_2 - m_2\mathbf{p}_3)/(m_2 + m_3)$, where $\mathbf{p}_j$ (m_j) with $j = 1$, 2, and 3 are the momentum vectors measured in the laboratory frame (the masses) of the first, second, and third fragments, respectively.

III. RESULTS AND DISCUSSION

Figure 1 presents a part of the triple-ion coincidence TOF map for the fragmentation of $C_3H_6^{3+}$ trications induced by 1-MeV/u C^{4+} ion collisions. The horizontal axis is the sum of the TOFs of the first and second detected ions, and the TOF of

the third fragment ion is along the vertical axis. In this map, four structures surrounded by red elliptical lines are identified to result from the complete three-body fragmentation of $C_3H_6^{3+}$, which are referred to as channels I–IV as follows:

$$C_3H_6^{3+} \rightarrow H^+ + CH_2^+ + C_2H_3^+ \quad \text{(channel I)},$$

$$C_3H_6^{3+} \rightarrow H^+ + CH_3^+ + C_2H_2^+ \quad \text{(channel II)},$$

$$C_3H_6^{3+} \rightarrow H^+ + H_2^+ + C_3H_3^+ \quad \text{(channel III)},$$

$$C_3H_6^{3+} \rightarrow H_2^+ + CH_2^+ + C_2H_2^+ \quad \text{(channel IV)}.$$

Besides the above identified three-body dissociation channels, the other structures in the coincidence TOF map are attributed to many-body fragmentation processes with the undetected fragment(s). The four fully measured three-body fragmentation channels of $C_3H_6^{3+}$ will be the focus of discussion in this work.

As depicted in Fig. 1, it is evident that channels I and II are the preferred pathways for the three-body dissociation of $C_3H_6^{3+}$. These two channels are formed via the breakage of both CH and CC bonds. Besides bond breaking, channels III and IV also require hydrogen atom displacement and hydrogen-hydrogen (HH) bond formation to produce H_2^+, hence their relatively small cross sections. To largely exclude the random coincidence events, the momentum sum in each dimension of three coincidence fragments is limited to lie within ±8 a.u. Since the complete collection of recoil ions is affected by the extraction field, during data analysis we limited the angle between the momentum of the lightest fragment (i.e., H^+ for channels I–III and H_2^+ for channel IV) and the TOF axis to be less than 40° in each channel to avoid the energetic ion losses. Under this condition and the assumption that the emission angles of the ions are isotropic, the relative branching ratios for channels I–IV are estimated to be ∼47%, ∼35%, ∼6%, and ∼12%, respectively. These ratios have a margin of error of about 15%, which is mainly due to the detection efficiency and statistical errors.

Subsequent to the identification of fragmentation channels, the kinetic energy of each ionic fragment and thus the KERs of the channels considered can be determined by the COLTRIMS technique. Figure 2 shows the KER distributions of fragmentation channels I–IV, and the uncertainties presented as vertical error bars are mainly from the data statistics. The broad distribution of impact parameters in ion-molecule collisions populates multiple electronic states and transfers a wide vibrational energy, leading to a broad KER distribution range of 8–18 eV. The KER distributions of channels I, II, and IV peak at ∼13.0 eV, while that of channel III peaks at ∼12.2 eV. This is due to the fact that compared with channel III only involving CH bond breaking, more kinetic energy could be released in the cleavage of CC bond involved in channels I, II, and IV. Such KER differences between the CH and CC bond-breaking channels were also found in previous works [41,44].

In the following sections we analyze the fragmentation mechanism of the four channels based on the momentum correlation of the resultant fragments. It should be noted that hydrogen atoms can exhibit significant mobility during fragmentation, leading to processes such as H or H_2 roaming

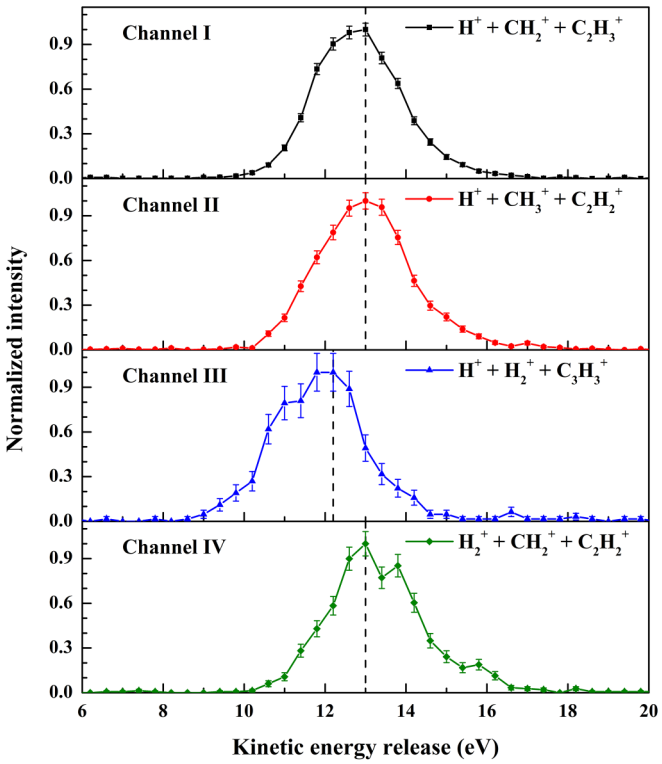

FIG. 2. KER distributions of four three-body fragmentation channels for $C_3H_6^{3+}$: (I) $H^+ + CH_2^+ + C_2H_3^+$, (II) $H^+ + CH_3^+ + C_2H_2^+$, (III) $H^+ + H_2^+ + C_3H_3^+$, and (IV) $H_2^+ + CH_2^+ + C_2H_2^+$. The vertical black dashed lines mark the peaks of the KER distributions.

[14–16]; the detailed structures or transient configurations of intermediates cannot be uniquely determined from the present data; and possible hydrogen migration or roaming processes cannot be excluded. Therefore, in the present experiment, only the final ionic fragments are directly measured, while the intermediate fragments are deduced.

A. Fragmentation channel $H^+ + CH_2^+ + C_2H_3^+$

Figures 3(a) and 3(b) present the Dalitz plot and Newton diagram of the fragmentation channel I. As can be seen, there are two momentum correlation patterns marked as regions A and B, respectively. In a sequential fragmentation process, the momentum distributions of the ions produced in the second Coulomb explosion process are no longer related to the Coulomb field in the first step. Considering the chain structure of propene, the proton and CH_2^+ fragments could be emitted first through the cleavage of one CH bond and the CC double bond, respectively. Thus, the stripelike regions A and B in the Dalitz plot are attributed to the following two-step sequential fragmentation processes:

$$C_3H_6^{3+} \rightarrow H^+ + C_3H_5^{2+}$$
$$\rightarrow H^+ + CH_2^+ + C_2H_3^+ \quad \text{(process Ia)},$$

$$C_3H_6^{3+} \rightarrow CH_2^+ + C_2H_4^{2+}$$
$$\rightarrow CH_2^+ + H^+ + C_2H_3^+ \quad \text{(process Ib)}.$$

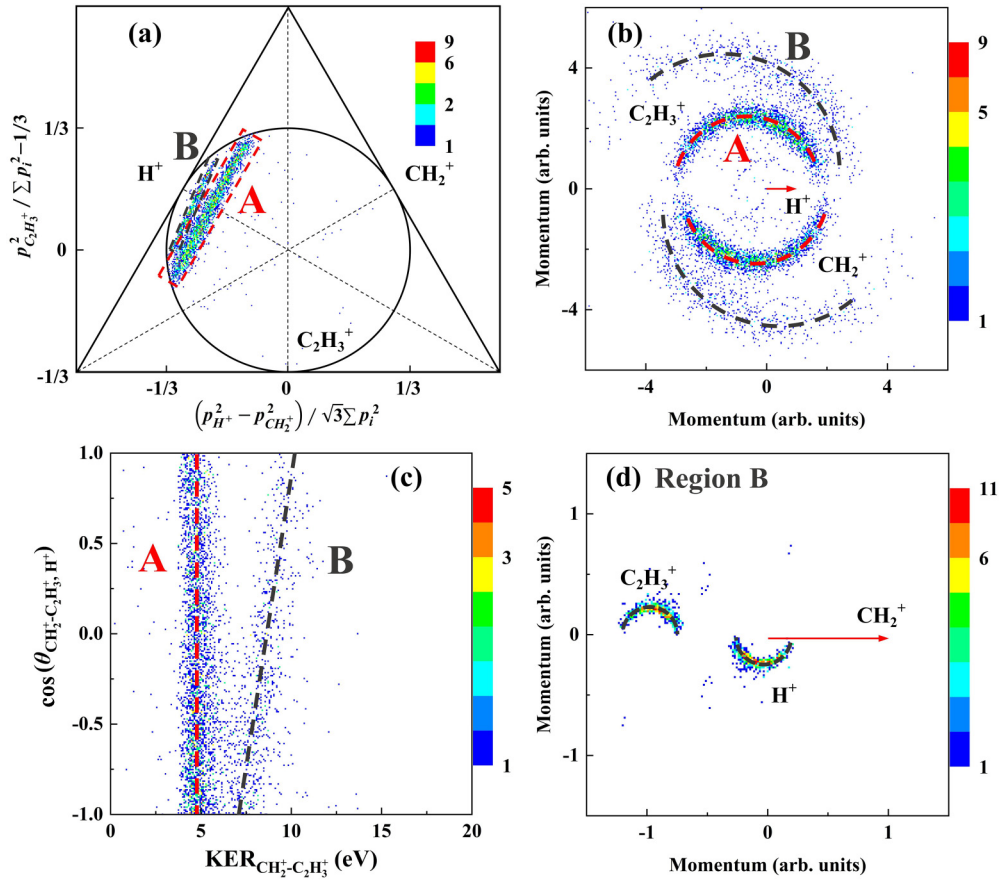

FIG. 3. (a) Dalitz plot and (b) Newton diagram normalized to the momentum of H^+ (red arrow) for the $H^+ + CH_2^+ + C_2H_3^+$ channel. The fragmentation events located at different regions are marked by A and B. (c) Native frame plot by assuming sequential fragmentation of $C_3H_6^{3+}$ via $H^+ + C_3H_5^{2+}$. (d) Newton diagram normalized to the momentum of CH_2^+ (red arrow) for the events in the inclined distribution in (c).

The distribution of region A is parallel to the H^+ side, that is, the momentum of the proton is independent of the momenta variations of CH_2^+ and $C_2H_3^+$, which indicates that the fragmentation results from the two-step sequential process Ia. The proton is emitted in the first step and then the $C_3H_5^{2+}$ dissociates to CH_2^+ and $C_2H_3^+$ ions. When the momentum vector of the CH_2^+ fragment obtained in the second Coulomb explosion fragmentation is parallel, perpendicular, or antiparallel to the vector of the intermediate $C_3H_5^{2+}$, the corresponding fragmentation events are located at the bottom, middle, or top of region A in Fig. 3(a). In the Newton diagram shown in Fig. 3(b), two complete semicircular structures marked by red dashed lines also indicate a sequential fragmentation mechanism with a proton emitted in the first step.

In addition, the distribution of region B exhibits a weaker circular structure in the Newton diagram as shown in Fig. 3(b), indicating a different sequential dissociation process occurring in this channel. Given the difficulty in defining a nontrivial cut in either the Dalitz plot or the Newton diagram, the native frame plot assuming sequential fragmentation of $C_3H_5^{2+}$ being the intermediate is shown in Fig. 3(c). The uniform distribution along the red dashed line corresponds to process Ia, which can be easily separated from the inclined distribution marked by the gray dashed line. To further identify the corresponding mechanism of the events in the inclined distribution, we plot the Newton diagram in Fig. 3(d) where the unit vector is set to the momentum of CH_2^+. The presence of two semicircular signatures identifies CH_2^+ as the first dissociation product, and the H^+ and $C_2H_3^+$ ions are subsequently produced in the second step. Thus, it is confirmed that the fragmentation in region B corresponds to the sequential fragmentation process Ib in which the CC bond breaks first before the CH bond breaking.

B. Fragmentation channel $H^+ + CH_3^+ + C_2H_2^+$

Figures 4(a) and 4(b) present the Dalitz plot and Newton diagram of channel II, which exhibit structures very similar to those of the $H^+ + CH_2^+ + C_2H_3^+$ channel. Two stripelike regions C and D are observed in the Dalitz plot, and two pairs of semicircular structures can also be seen in the Newton diagram. This indicates that there are two distinct sequential fragmentation processes contributing to this channel.

In the Dalitz plot shown in Fig. 4(a), the distribution of region C is parallel to the H^+ side, which is the same as process Ia and indicates that the fragmentation results from the two-step sequential process

$$C_3H_6^{3+} \rightarrow H^+ + C_3H_5^{2+}$$
$$\rightarrow H^+ + CH_3^+ + C_2H_2^+ \quad \text{(process IIa)}.$$

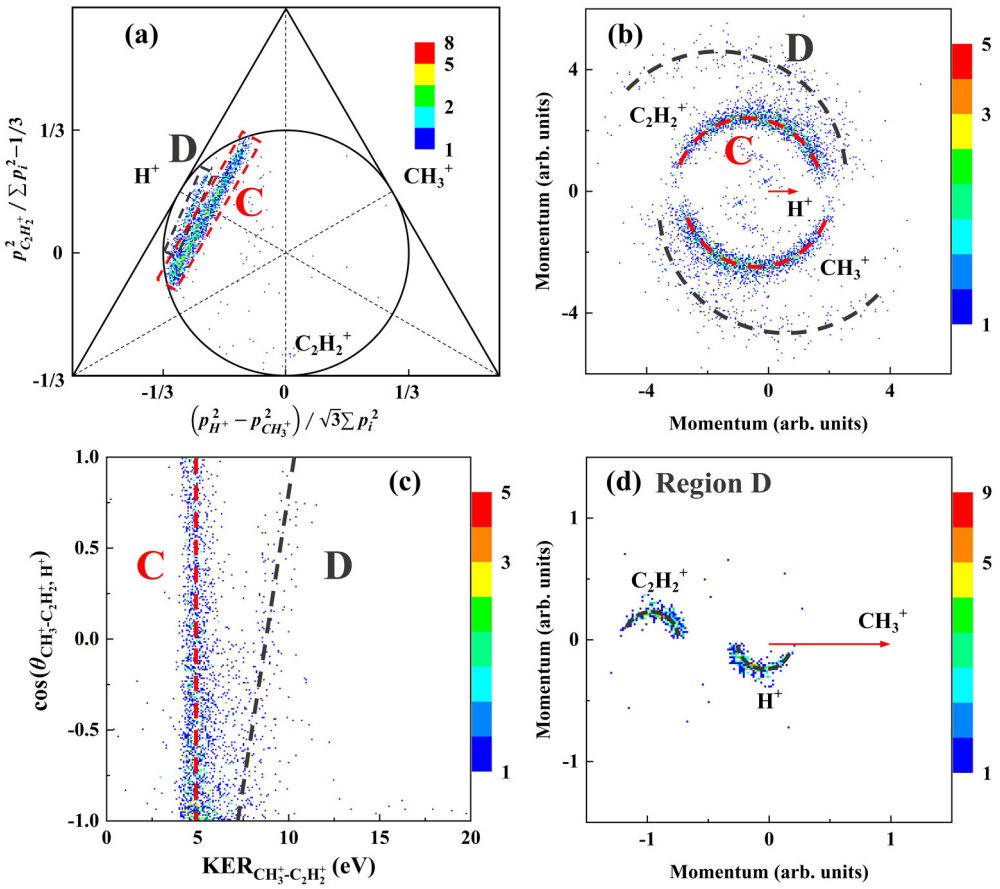

FIG. 4. (a) Dalitz plot and (b) Newton diagram normalized to the momentum of H^+ (red arrow) for the $H^+ + CH_3^+ + C_2H_2^+$ channel. The fragmentation events located at different regions are marked by C and D. (c) Native frame plot by assuming sequential fragmentation of $C_3H_6^{3+}$ via $H^+ + C_3H_5^{2+}$. (d) Newton diagram normalized to the momentum of CH_3^+ (red arrow) for the events in the inclined distribution in (c).

In this sequential process, the CH bond breaks prior to the CC bond, i.e., the proton is emitted in the first step, and then the $C_3H_5^{2+}$ dissociates to CH_3^+ and $C_2H_2^+$ ions. The sequential process IIa with the proton emitted in the first step is also supported by the two complete semicircular structures marked by red dashed lines in the Newton diagram shown in Fig. 4(b).

Note that a weak stripelike region D appears in the Dalitz plot marked by the gray rectangle in Fig. 4(a), and the events in region D correspond to the two weaker semicircular structures in the Newton diagram marked by gray dashed lines in Fig. 4(b). These features indicate that another sequential fragmentation process alternative to process IIa occurred. Like that CH_2^+ emitted first in channel Ib, the CH_3^+ fragment could also be emitted first in channel II through direct cleavage of the CC single bond in propene. The native frame plot is employed to make the separation of regions C and D easier, where the sequential process is assumed to proceed via $H^+ + C_3H_5^{2+}$, as shown in Fig. 4(c). Then Fig. 4(d) presents the Newton diagram normalized to the momentum of CH_3^+ for the inclined distribution along the gray dashed line in Fig. 4(c). Two semicircular structures are typical features of the sequential fragmentation process with CH_3^+ emitted in the first step while H^+ and $C_2H_2^+$ are produced in a following step as follows:

$$C_3H_6^{3+} \rightarrow CH_3^+ + C_2H_3^{2+}$$
$$\rightarrow CH_3^+ + H^+ + C_2H_2^+ \quad \text{(process IIb)}.$$

The weak intensity of region D in Fig. 4 indicates that process IIb with CC bond breaking prior to CH bond breaking is not prone to occur in this channel.

Moreover, the relative branching ratio of channel I with one CH_2^+ fragment (~47%) is higher than that of channel II with one CH_3^+ fragment (~35%). This may be attributed to the fact that the CH_2^+ fragments could be produced not only through the CC double-bond breaking but also in the case that the CC and CH bonds break from the same carbon atom in the CH_3 group, while the CH_3^+ fragments could only be produced by the CC single-bond breaking unless hydrogen migration occurs.

C. Fragmentation channel $H^+ + H_2^+ + C_3H_3^+$

Besides channels I and II that could be readily created through bond breaking, channels III and IV involving production of the molecular ion H_2^+ were also observed in the present study. The H_2^+ ion could be formed by two hydrogen atoms either from the same C atom (CH_2 or CH_3 group)

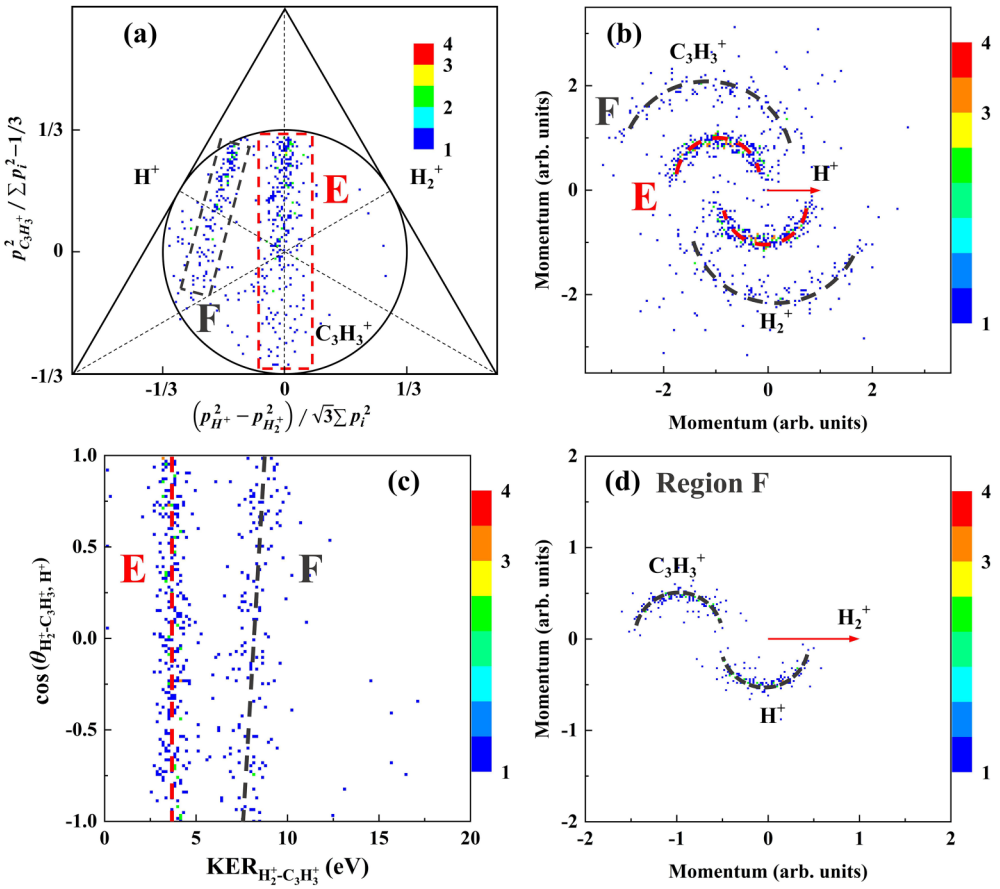

FIG. 5. (a) Dalitz plot and (b) Newton diagram normalized to the momentum of H^+ (red arrow) for the $H^+ + H_2{}^+ + C_3H_3{}^+$ channel. The fragmentation events located at different regions are marked by E and F. (c) Native frame plot by assuming sequential fragmentation of $C_3H_6^{3+}$ via $H^+ + C_3H_5{}^{2+}$. (d) Newton diagram normalized to the momentum of $H_2{}^+$ (red arrow) for the events in the inclined distribution in (c).

or from different C atoms (probably involving hydrogen migration). However, such details of fragmentation dynamics require further quantum chemical calculations. Here we focus on clarifying the dissociation mechanisms of these channels.

The Dalitz plot and Newton diagram of channel III are shown in Figs. 5(a) and 5(b), respectively. Two stripelike structures marked as regions E and F in the Dalitz plot and two pairs of semicircular structures in the Newton diagram can be clearly seen. As discussed in channels I and II, these features are signatures of two different sequential fragmentation processes.

To more clearly identify these two processes, the native frame plot assuming sequential fragmentation involving the $C_3H_5{}^{2+}$ intermediate is shown in Fig. 5(c). The uniform distribution centered around 3.9 eV along the red dashed line indicates the sequential process with the $C_3H_5{}^{2+}$ intermediate as follows:

$$C_3H_6^{3+} \rightarrow H^+ + C_3H_5^{2+}$$
$$\rightarrow H^+ + H_2^+ + C_3H_3^+ \quad \text{(process IIIa)}.$$

This process is further confirmed by the semicircular structures marked by the red dashed semicircles in the Newton diagram normalized to the momentum of H^+ as shown in Fig. 5(b). In the first step, the $C_3H_6^{3+}$ trication breaks into the H^+ and the metastable $C_3H_5{}^{2+}$ ion. After rotation, the intermediate ion dissociates into the final products $H_2{}^+$ and $C_2H_3{}^+$ in the second step.

In addition to the uniform distribution parallel to the $\cos\theta$ axis, the inclined distribution marked by the gray dashed line in Fig. 5(c) corresponds to another sequential process. To see this process more directly, the Newton diagram for the events in the inclined distribution, where the unit vector is set to the momentum of $H_2{}^+$, is plotted in Fig. 5(d). Two apparent semicircular features reveal $H_2{}^+$ as the fragment from the first dissociation step, and H^+ and $C_3H_3{}^+$ ions are, subsequently, produced in the second step. This confirms secondary sequential fragmentation process in channel III as follows:

$$C_3H_6^{3+} \rightarrow H_2^+ + C_3H_4^{2+}$$
$$\rightarrow H_2^+ + H^+ + C_3H_3^+ \quad \text{(process IIIb)}.$$

In this process, bond rearrangement occurs first to form the H_2 radical before the Coulomb explosion.

D. Fragmentation channel $H_2{}^+ + CH_2{}^+ + C_2H_2{}^+$

For channel IV, the Dalitz plot and Newton diagram are shown in Figs. 6(a) and 6(b), respectively. As can be seen from the Newton diagram, the gathering island structure marked as region G is brighter than semicircular structures, which is a typical feature of concerted fragmentation process, although

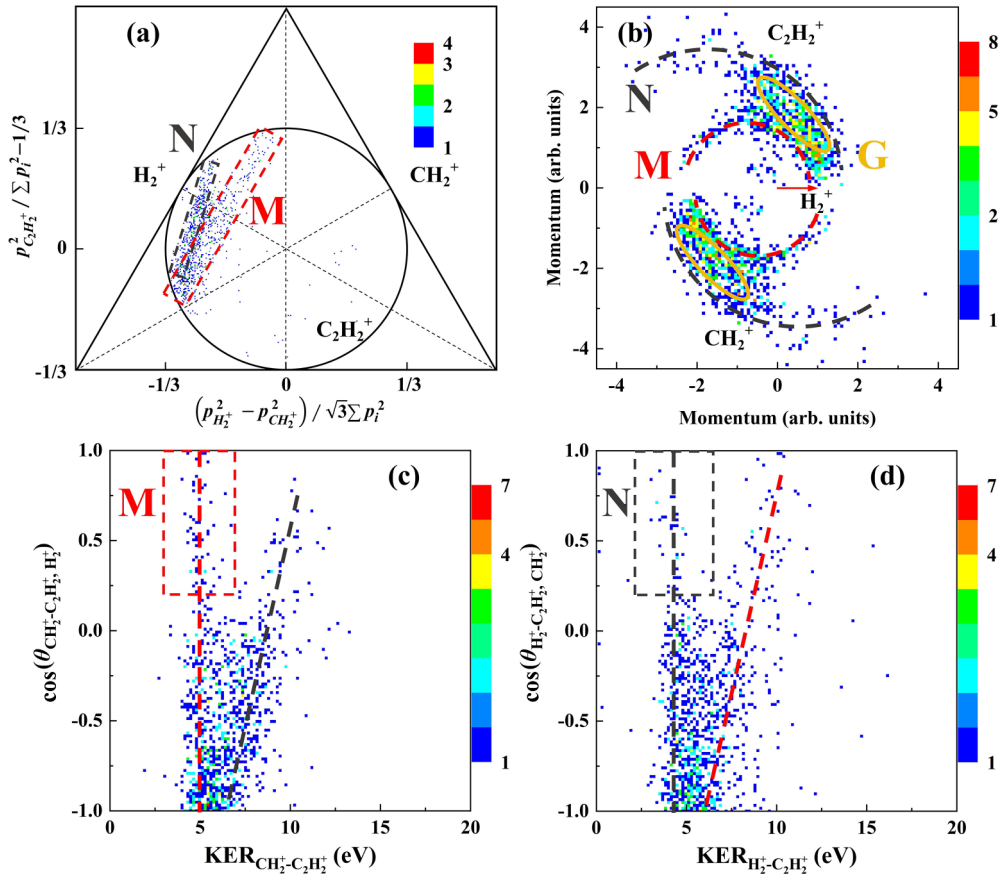

FIG. 6. (a) Dalitz plot and (b) Newton diagram normalized to the momentum of H_2^+ (red arrow) for the $H_2^+ + CH_2^+ + C_2H_2^+$ channel. The fragmentation events located at different regions are marked by G, M, and N. (c) Native frame plot by assuming sequential fragmentation of $C_3H_6^{3+}$ via $H_2^+ + C_3H_4^{2+}$. The events in the red dashed rectangle are exclusively from the sequential process IVb. (d) Native frame plot by assuming sequential fragmentation of $C_3H_6^{3+}$ via $CH_2^+ + C_2H_4^{2+}$. The events in the gray dashed rectangle are exclusively from the sequential process IVc.

this process cannot be clearly distinguished in the Dalitz plot due to its overlap with stripelike structures. The corresponding pathway for the concerted fragmentation process is as follows:

$$C_3H_6^{3+} \rightarrow H_2^+ + CH_2^+ + C_2H_2^+ \quad \text{(process IVa)}.$$

Besides that, as discussed for channels I–III, two stripelike structures marked as regions M and N in the Dalitz plot are signatures of the sequential dissociation processes. Two pairs of semicircular patterns in the Newton diagram marked by red and gray dashed lines also confirm two sequential mechanisms. Additionally, the native frame plot assuming $C_3H_4^{2+}$ to be the intermediate, as a function of the distribution $\cos(\theta_{CH_2^+\text{–}C_2H_2^+,H_2^+})$ and the KER in the second step of the $C_3H_4^{2+}$ dissociation, is presented in Fig. 6(c) to identify the fragmentation sequences. A vertical distribution along the $\cos\theta$ axis means that the KER from the intermediate fragment $C_3H_4^{2+}$ is independent of the rotation angle relative to the first emitted H_2^+ ion, suggesting that the sequential breakup process is as follows:

$$\begin{aligned} C_3H_6^{3+} &\rightarrow H_2^+ + C_3H_4^{2+} \\ &\rightarrow H_2^+ + CH_2^+ + C_2H_2^+ \quad \text{(process IVb)}. \end{aligned}$$

Similar to the features of process IIIb observed in Fig. 5(c), the inclined distribution in the native frame plot shown in Fig. 6(c) corresponds to another sequential fragmentation process in channel IV. It is worth noting that CH_2^+ can also be emitted in the first step through the breaking of the CC double bond, which readily occurs in this study as discussed earlier. To further confirm another sequential process, the native frame plot assuming $C_2H_4^{2+}$ to be the intermediate is presented in Fig. 6(d). It can be seen that the vertical distribution along the gray dashed line corresponds to the sequential fragmentation process

$$\begin{aligned} C_3H_6^{3+} &\rightarrow CH_2^+ + C_2H_4^{2+} \\ &\rightarrow CH_2^+ + H_2^+ + C_2H_2^+ \quad \text{(process IVc)}, \end{aligned}$$

which is responsible for the formation of channel IV.

E. Relative contributions

Finally, according to the native frame plots of four channels, the branching ratios of different fragmentation mechanisms are analyzed and listed in Table I. The uncertainties for channels I–III are mainly contributed by the statistical errors. In the native frame plots of channel IV [Figs. 6(c) and 6(d)], the uniform distributions from processes IVb and

TABLE I. Branching ratios of different fragmentation processes for the channels considered.

Channel	Branching ratio		
	Concerted	Sequential	
$H^+ + CH_2^+ + C_2H_3^+$		Ia: 78.8% ± 1.3%	Ib: 21.2% ± 0.3%
$H^+ + CH_3^+ + C_2H_2^+$		IIa: 82.5% ± 1.7%	IIb: 17.5% ± 0.4%
$H^+ + H_2^+ + C_3H_3^+$		IIIa: 62.6% ± 2.9%	IIIb: 37.4% ± 1.7%
$H_2^+ + CH_2^+ + C_2H_2^+$	IVa: 76.7% ± 3.1%	IVb: 14.0% ± 1.4%	IVc: 9.3% ± 1.3%

IVc (within the red and gray dashed rectangles, respectively) are clearly separated from overlapping areas among three fragmentation mechanisms, so the events in the rectangles are extracted to deduce the branching ratios of channel IV. The uncertainty for channel IV includes both statistical and systematic components. The systematic contribution arises from the estimation of the total sequential yield using sparse sequential data and is conservatively quantified by varying the selection gate position.

As listed in Table I, under the present 1-MeV/u C^{4+} impact corresponding to the velocity of 6.32 a.u., processes Ia and IIa with the proton emitted in the first step, i.e., the CH bonds breaking prior to CC bonds breaking, make the major contributions to channels I and II. Also studied were these two three-body fragmentation channels of cyclopropane (an isomer of propene) induced by 5.8-MeV/u Ni^{19+} ion collisions [52] with a velocity of 15.23 a.u. Both Ref. [52] and the present study employ impact energies in the several-MeV/u region, where postcollisional ionization is the dominant contribution [56]. Both isomers, propene and cyclopropane, show similar fragmentation mechanisms, i.e., two distinct sequential processes are distinguished in each channel depending on the breaking sequence of the CH and CC bonds. For channel I, $H^+ + CH_2^+ + C_2H_3^+$, different from cyclopropane, where the contributions of two sequential pathways are found to be comparable, for propene, the contribution of process Ia is much larger than that of process Ib. Additionally, for channel II, $H^+ + CH_3^+ + C_2H_2^+$, the branching ratios of two sequential pathways of cyclopropane [52] are in agreement with those of propene in this study, where the sequential process with CH bond breaking in the first step followed by CC bond breaking (i.e., process IIa) contributes significantly to this channel. Note that for cyclopropane, the channel $H^+ + CH_3^+ + C_2H_2^+$ involves proton migration and process IIa could be dominant, assuming that the first step of sequential fragmentation is faster than proton migration [52], but for propene, two sequential pathways occurring in channel II only depend on the sequence of CH and CC single-bond breaking, and the sequential process with CH bond breaking in the first step makes the major contribution here. Such differences between the two isomers indicate apparent isomer effects. However, the discrepancies in branching ratios may not stem exclusively from isomer effects, as the employment of different projectiles may also contribute significantly.

For channels III, $H^+ + H_2^+ + C_3H_3^+$, and IV, $H_2^+ + CH_2^+ + C_2H_2^+$, involving the H_2 formation, as listed in Table I, the major contributions are the sequential process IIIa with H^+ emitted in the first step and the concerted process IVa, respectively. Although the H_2 formation involves hydrogen displacement and HH bond formation, it still plays a role and competes with the molecular fragmentation in channels III and IV. This could be attributed to the similar timescales of the H_2 formation process and the first step in the sequential fragmentation process. The H_2 formation can take place on timescales ranging from tens to hundreds of femtoseconds [16,57], while the timescale of the first step in the sequential fragmentation is estimated to be around tens of femtoseconds [58,59]. Furthermore, H_2 formation is generally accompanied by ultrafast hydrogen migration occurring on sub-100-fs timescales [60–62], which may occur following propene triple ionization and finally enable fragmentation pathways featuring H_2^+ emission in the first step. Therefore, the occurrence of either process IIIa or IIIb in channel III, $H^+ + H_2^+ + C_3H_3^+$, depends on the step in which the H_2^+ can be generated. If the H_2 formation occurs faster than the molecular fragmentation, the concerted process IVa and the sequential process IVb with H_2^+ emitted first in channel IV, $H_2^+ + CH_2^+ + C_2H_2^+$, are more probable.

IV. CONCLUSION

In summary, the three-body fragmentation dynamics of propene trications $[(H_3C–CH{=}CH_2)^{3+}]$ induced by 1-MeV/u C^{4+} ion impact was studied employing the COLTRIMS technique. The complete dissociation channels, i.e., (I) $H^+ + CH_2^+ + C_2H_3^+$, (II) $H^+ + CH_3^+ + C_2H_2^+$, (III) $H^+ + H_2^+ + C_3H_3^+$, and (IV) $H_2^+ + CH_2^+ + C_2H_2^+$, were identified through the triple-ion coincidence TOF map. Fragmentation mechanisms for all four channels were elucidated through Dalitz plots, Newton diagrams, and the native frame method. Analysis revealed that each channel possesses two distinct sequential processes; notably, channel IV additionally features a concerted process. Branching ratios of different fragmentation mechanisms were determined for each channel.

For channels I and II, compared to the previous results of cyclopropane trications $[(H_2C–CH_2–CH_2)^{3+}]$ produced by 5.8-MeV/u Ni^{19+} ion impact [52], the sequence of CH and CC bond cleavage causes similar fragmentation mechanisms for both isomers. In the fragmentation of cyclopropane, two sequential pathways contributed comparably to channel I while proton migration involved in channel II [52], whereas in the fragmentation of propene, both sequential processes with CH bond cleavage preceding CC bond cleavage predominate in channels I and II. The structural difference between two isomers, as well as the distinct projectiles used in two experiments, may affect the relative contributions of

fragmentation pathways. For channels III and IV, which involve H_2^+ generation in the present study, the sequential process with initial H^+ emission and the concerted process are the dominant contributors to the two channels, respectively. Though hydrogen displacement and HH bond formation are required for H_2^+ production, fragmentation pathways featuring H_2^+ emission in the first step contribute to channels III and IV. This suggests potential kinetic competition between the H_2 formation and the molecular fragmentation, which could be ascribed to their comparable timescales [16,57–59]. To better understand H_2^+ production in the fragmentation of propene tricications, quantum chemical calculations could be performed, and questions, e.g., whether the two hydrogen atoms forming the H_2 molecule originate from the same C atom or different C atoms, might be addressed more thoroughly.

ACKNOWLEDGMENTS

This work was supported by the National Natural Science Foundation of China (Grants No. 12304275 and No. 12374234), the National Key R&D Program of China (Grant No. 2022YFA1602500), and the Sichuan Science and Technology Program (Grants No. 2025ZNSFSC0883 and No. 2025NSFJQ0042).

DATA AVAILABILITY

The data that support the findings of this article are not publicly available. The data are available from the authors upon reasonable request.

[1] S. Maclot, R. Delaunay, D. G. Piekarski, A. Domaracka, B. A. Huber, L. Adoui, F. Martín, M. Alcamí, L. Avaldi, P. Bolognesi, S. Díaz-Tendero, and P. Rousseau, Determination of energy-transfer distributions in ionizing ion-molecule collisions, Phys. Rev. Lett. **117**, 073201 (2016).

[2] N. Neumann, D. Hant, L. P. H. Schmidt, J. Titze, T. Jahnke, A. Czasch, M. S. Schöffler, K. Kreidi, O. Jagutzki, H. Schmidt-Böcking, and R. Dörner, Fragmentation dynamics of CO_2^{3+} investigated by multiple electron capture in collisions with slow highly charged ions, Phys. Rev. Lett. **104**, 103201 (2010).

[3] E. Alizadeh, T. M. Orlando, and L. Sanche, Biomolecular damage induced by ionizing radiation: The direct and indirect effects of low-energy electrons on DNA, Annu. Rev. Phys. Chem. **66**, 379 (2015).

[4] Y. Gao, A. D. Skitnevskaya, E. Wang, H. Yuan, X. Ren, H. Lin, Z. Yan, S. Zhang, S. Gu, B. Yang, F. Fang, S. Yan, D. Guo, X. Zhu, D. Zhao, C. Shao, Z. Huang, X. Xue, X. Hao, J. Zhou, *et al.*, Damaging intermolecular relaxation processes initiated by heavy-ion irradiation of hydrated biomolecules, Phys. Rev. X **15**, 011053 (2025).

[5] W. D. Geppert and M. Larsson, Experimental investigations into astrophysically relevant ionic reactions, Chem. Rev. **113**, 8872 (2013).

[6] A. G. G. M. Tielens, The molecular universe, Rev. Mod. Phys. **85**, 1021 (2013).

[7] D. Reiter and R. K. Janev, Hydrocarbon collision cross sections for magnetic fusion: The methane, ethane and propane families, Contrib. Plasma Phys. **50**, 986 (2010).

[8] K. Bartschat and M. J. Kushner, Electron collisions with atoms, ions, molecules, and surfaces: Fundamental science empowering advances in technology, Proc. Natl. Acad. Sci. USA **113**, 7026 (2016).

[9] C. Wu, C. Wu, D. Song, H. Su, Y. Yang, Z. Wu, X. Liu, H. Liu, M. Li, Y. Deng, Y. Liu, L.-Y. Peng, H. Jiang, and Q. Gong, Nonsequential and sequential fragmentation of CO_2^{3+} in intense laser fields, Phys. Rev. Lett. **110**, 103601 (2013).

[10] A. Khan, L. C. Tribedi, and D. Misra, Observation of a sequential process in charge-asymmetric dissociation of $CO_2^{q+}(q = 4, 5)$ upon the impact of highly charged ions, Phys. Rev. A **92**, 030701(R) (2015).

[11] J. Rajput, T. Severt, B. Berry, B. Jochim, P. Feizollah, B. Kaderiya, M. Zohrabi, U. Ablikim, F. Ziaee, K. Raju P., D. Rolles, A. Rudenko, K. D. Carnes, B. D. Esry, and I. Ben-Itzhak, Native frames: Disentangling sequential from concerted three-body fragmentation, Phys. Rev. Lett. **120**, 103001 (2018).

[12] C.-M. Tseng, M. Fushitani, A. Matsuda, and A. Hishikawa, Coincidence momentum imaging of four- and three-body Coulomb explosion of formaldehyde in ultrashort intense laser fields, J. Electron Spectrosc. Relat. Phenom. **228**, 25 (2018).

[13] E. Wang, M. Gong, Z. Shen, X. Shan, X. Ren, A. Dorn, and X. Chen, Fragmentation dynamics of CS_2 in collisions with 1.0 keV electrons, J. Chem. Phys. **149**, 204301 (2018).

[14] D. Mishra, A. C. LaForge, L. M. Gorman, S. Díaz-Tendero, F. Martín, and N. Berrah, Direct tracking of H_2 roaming reaction in real time, Nat. Commun. **15**, 6656 (2024).

[15] T. Endo, S. P. Neville, V. Wanie, S. Beaulieu, C. Qu, J. Deschamps, P. Lassonde, B. E. Schmidt, H. Fujise, M. Fushitani, A. Hishikawa, P. L. Houston, J. M. Bowman, M. S. Schuurman, F. Légaré, and H. Ibrahim, Capturing roaming molecular fragments in real time, Science **370**, 1072 (2020).

[16] Y. Zhang, B. Ren, C.-L. Yang, L. Wei, B. Wang, J. Han, W. Yu, Y. Qi, Y. Zou, L. Chen, E. Wang, and B. Wei, Formation of H_3^+ from ethane dication induced by electron impact, Commun. Chem. **3**, 160 (2020).

[17] L. Wei, C.-S. Lam, Y. Zhang, B. Ren, J. Han, B. Wang, Y. Zou, L. Chen, K.-C. Lau, and B. Wei, Isomerization dynamics in the symmetric and asymmetric fragmentation of ethane dications, J. Phys. Chem. Lett. **12**, 5789 (2021).

[18] J. Yadav, C. P. Safvan, P. Bhatt, P. Kumari, A. Kumar, and J. Rajput, Hydrogen migration in triply charged acetylene, J. Chem. Phys. **156**, 141101 (2022).

[19] J. Ullrich, R. Moshammer, A. Dorn, R. Dörner, L. P. H. Schmidt, and H. Schmidt-Böcking, Recoil-ion and electron momentum spectroscopy: Reaction-microscopes, Rep. Prog. Phys. **66**, 1463 (2003).

[20] I. Ben-Itzhak, K. D. Carnes, S. G. Ginther, D. T. Johnson, P. J. Norris, and O. L. Weaver, Fragmentation of CH_4 caused by fast-proton impact, Phys. Rev. A **47**, 3748 (1993).

[21] R. Flammini, M. Satta, E. Fainelli, G. Alberti, F. Maracci, and L. Avaldi, The role of the methyl ion in the fragmentation of CH_4^{2+}, New J. Phys. **11**, 083006 (2009).

[22] Y. Zhang, T. Jiang, L. Wei, D. Luo, X. Wang, W. Yu, R. Hutton, Y. Zou, and B. Wei, Three-body fragmentation of methane dications produced by slow Ar^{8+}-ion impact, Phys. Rev. A **97**, 022703 (2018).

[23] C. Cao, M. Li, K. Guo, Z. Li, Y. Liu, Y. Liu, K. Liu, Y. Zhou, and P. Lu, Intensity-dependent three-body Coulomb explosion of methane in femtosecond laser pulses, Phys. Rev. A **109**, 023115 (2024).

[24] R. Thissen, J. Delwiche, J. M. Robbe, D. Duflot, J. P. Flament, and J. H. D. Eland, Dissociations of the ethyne dication $C_2H_2^{2+}$, J. Chem. Phys. **99**, 6590 (1993).

[25] N. Saito, M. Nagoshi, M. Machida, I. Koyano, A. De Fanis, and K. Ueda, Intra-molecular H_2^+ formation in the core-excited HCCH probed by multiple-ion coincidence momentum imaging, Chem. Phys. Lett. **393**, 295 (2004).

[26] A. Hishikawa, A. Matsuda, M. Fushitani, and E. J. Takahashi, Visualizing recurrently migrating hydrogen in acetylene dication by intense ultrashort laser pulses, Phys. Rev. Lett. **99**, 258302 (2007).

[27] S. De, J. Rajput, A. Roy, P. N. Ghosh, and C. P. Safvan, Ion-induced dissociation dynamics of acetylene, Phys. Rev. A **77**, 022708 (2008).

[28] R. Flammini, M. Satta, E. Fainelli, and L. Avaldi, Effect of the charge localization in the $C^+ - H^+$ fragmentation pathway of the ethyne dication, Phys. Rev. A **83**, 014501 (2011).

[29] T. Jiang, B. Wang, Y. Zhang, L. Wei, S. Chen, W. Yu, Y. Zou, L. Chen, and B. Wei, Three-fragment dissociation of $C_2H_2^{2+}$ and $C_2H_2^{3+}$ produced by slow-Ar^{8+}-ion impact, Phys. Rev. A **100**, 022705 (2019).

[30] Y. Wang, X. Shi, J. Zhou, S. Xu, D. Guo, S. Yan, X. Zhu, and X. Ma, Four-body Coulomb explosion of acetylene in collision with highly charged ions, Phys. Rev. A **101**, 042706 (2020).

[31] J. Yadav, C. P. Safvan, P. Bhatt, P. Kumari, J. Singh, and J. Rajput, Exploring three-body fragmentation of acetylene trication, J. Chem. Phys. **158**, 074302 (2023).

[32] Y. Gao, Y. Pan, S. Xu, K.-C. Lau, H. Yuan, Z. Yan, D. Guo, D. Zhao, X. Zhu, S. Yan, S. Zhang, Z. Xu, and X. Ma, Fragmentation dynamics of acetylene in collision with highly charged ions: Concerted and sequential breakage of CH and CC bonds, Phys. Rev. A **107**, 012811 (2023).

[33] S.-H. Lee, Y. T. Lee, and X. Yang, Dynamics of photodissociation of ethylene and its isotopomers at 157 nm: Branching ratios and kinetic-energy distributions, J. Chem. Phys. **120**, 10983 (2004).

[34] X. Xie, E. Lötstedt, S. Roither, M. Schöffler, D. Kartashov, K. Midorikawa, A. Baltuška, K. Yamanouchi, and M. Kitzler, Duration of an intense laser pulse can determine the breakage of multiple chemical bonds, Sci. Rep. **5**, 12877 (2015).

[35] B. Ren, Z. Xia, Y. Zhang, L. Wei, W. Yu, J. Han, B. Wang, Y. Zou, L. Chen, and B. Wei, Three-body fragmentation mechanism of $C_2H_4^{3+}$ produced by 18-keV/u Ne^{8+} impact, Phys. Rev. A **104**, 022811 (2021).

[36] H. Xu, T. Okino, and K. Yamanouchi, Tracing ultrafast hydrogen migration in allene in intense laser fields by triple-ion coincidence momentum imaging, J. Chem. Phys. **131**, 151102 (2009).

[37] H. Xu, T. Okino, and K. Yamanouchi, Ultrafast delocalization of hydrogen atoms in allene in intense laser fields, Appl. Phys. A **104**, 941 (2011).

[38] H. Xu, T. Okino, and K. Yamanouchi, Ultrafast hydrogen migration in allene in intense laser fields: Evidence of two-body Coulomb explosion, Chem. Phys. Lett. **469**, 255 (2009).

[39] T. Kusakabe, S. Satoh, H. Tawara, and M. Kimura, Observation of the isomer effect on charge transfer from C_3H_4 molecules (Allene and propyne) at keV energies, Phys. Rev. Lett. **87**, 243201 (2001).

[40] S. W. J. Scully, V. Senthil, J. A. Wyer, M. B. Shah, E. C. Montenegro, M. Kimura, and H. Tawara, Direct evidence of a strong isomer effect in electron-impact double ionization of C_3H_4, Phys. Rev. A **72**, 030701(R) (2005).

[41] Y. Li, S. Xu, D. Guo, S. Jia, X. Jiang, X. Zhu, and X. Ma, Two-body dissociation of C_3H_4 isomers investigated by 50 keV/u Ne^{8+} impact, J. Chem. Phys. **150**, 144311 (2019).

[42] H. Yuan, Z. Xu, S. Xu, C. Ma, Z. Zhang, D. Guo, X. Zhu, D. Zhao, S. Zhang, S. Yan, Y. Gao, R. Zhang, and X. Ma, Three-body fragmentation dynamics of CH_3CCH^{3+} investigated by 50-kev/u Ne^{8+} impact: Comparison with its isomer ion $CH_2CCH_2^{3+}$, Phys. Rev. A **105**, 022814 (2022).

[43] C. Ma, S. Xu, D. Zhao, D. Guo, S. Yan, W. Feng, X. Zhu, and X. Ma, Three-body fragmentation dynamics of $CH_2CCH_2^{3+}$ investigated by 50-keV/u Ne^{8+} impact, Phys. Rev. A **101**, 052701 (2020).

[44] Z. He, J. Wang, Y. Zhang, B. Wang, J. Han, B. Ren, L. Wei, Z. Xia, P. Ma, T. Meng, Y. Zou, Z. Hu, and B. Wei, Sequential deprotonation of the allene trication produced by 30-keV/u He^{2+} impact, Phys. Rev. A **105**, 022818 (2022).

[45] P. J. Richardson, J. H. D. Eland, and P. Lablanquie, Charge separation reactions of doubly charged benzene ions, Org. Mass Spectrom. **21**, 289 (1986).

[46] A. Matsuda, M. Fushitani, R. D. Thomas, V. Zhaunerchyk, and A. Hishikawa, Multiple explosion pathways of the deuterated benzene trication in 9-fs intense laser fields, J. Phys. Chem. A **113**, 2254 (2009).

[47] J. Zhou, Y. Li, Y. Wang, S. Jia, X. Xue, T. Yang, Z. Zhang, A. Dorn, and X. Ren, Ultrafast ring-opening fragmentation dynamics of $C_6H_6^{3+}$ induced by electron-impact ionization, Phys. Rev. A **104**, 032807 (2021).

[48] X. Yu, X. Zhang, X. Hu, X. Zhao, D. Ren, X. Li, P. Ma, C. Wang, Y. Wu, S. Luo, and D. Ding, Femtosecond time-resolved neighbor roles in the fragmentation dynamics of molecules in a dimer, Phys. Rev. Lett. **129**, 023001 (2022).

[49] S.-H. Lee, Y.-Y. Lee, Y. T. Lee, and X. Yang, Photodissociation dynamics of propene at 157.6 nm: Kinetic energy distributions and branching ratios, J. Chem. Phys. **119**, 827 (2003).

[50] S. Oghbaie, M. Gisselbrecht, E. P. Månsson, J. Laksman, C. Stråhlman, A. Sankari, and S. L. Sorensen, Dissociation of cyclopropane in double ionization continuum, Phys. Chem. Chem. Phys. **19**, 19631 (2017).

[51] D. L. Guo, K. Z. Lin, X. L. Zhu, R. T. Zhang, Y. Gao, D. M. Zhao, X. B. Zhu, S. F. Zhang, and X. Ma, Two- and three-body dissociations of C_3H_6 isomer dications investigated by 4 keV/u Ar^{8+} impact, J. Chem. Phys. **157**, 154309 (2022).

[52] K. Z. Lin, D. L. Guo, X. L. Zhu, D. M. Zhao, X. B. Zhu, X. Shan, S. F. Zhang, X. J. Chen, and X. Ma, Three-body fragmentation dynamics of the cyclopropane trication following 5.8-MeV/u Ni^{19+} impact, Phys. Rev. A **109**, 022817 (2024).

[53] M. L. Duan, Z. C. He, Z. H. He, L. Zhou, B. R. Wei, and Z. M. Hu, A cold target recoil-ion momentum spectroscopy for atomic and molecular reaction dynamics induced by ions at few-mev energies, IEEE Trans. Nucl. Sci. **72**, 2206 (2025).

[54] M. L. Duan, Z. C. He, Z. H. He, B. R. Wei, and Z. M. Hu, Fragmentation of CO_2^{2+} into $C^+ + O^+ + O$ in collisions with 1 MeV/u C^{4+} ions, Phys. Rev. A **112**, 062822 (2025).

[55] T. Severt, J. Rajput, B. Berry, B. Jochim, P. Feizollah, B. Kaderiya, M. Zohrabi, F. Ziaee, K. Raju P., D. Rolles, A. Rudenko, K. D. Carnes, B. D. Esry, and I. Ben-Itzhak, Native frames: An approach for separating sequential and concerted three-body fragmentation, Phys. Rev. A **110**, 053104 (2024).

[56] C. C. Montanari and J. E. Miraglia, Multiple ionization of argon by helium ions, J. Phys. B: At. Mol. Opt. Phys. **49**, 175203 (2016).

[57] S. Jia, J. Zhou, C. Zhang, T. Yang, J. Xu, X. Xue, X. Hao, Q. Zeng, and X. Ren, Investigation of H_2 formation in electron-impact double ionization and fragmentation of tetrahydrofuran by multiparticle coincidence momentum imaging and *ab initio* calculations, Phys. Rev. A **109**, 052821 (2024).

[58] H. J. Yang, E. Wang, W. X. Dong, M. Gong, Z. Shen, Y. Tang, X. Shan, and X. Chen, Ultrafast fragmentation dynamics of triply charged carbon dioxide: Vibrational-mode-dependent molecular bond breakage, Phys. Rev. A **97**, 052703 (2018).

[59] S. Ohmura, K. Nagaya, F. Shimojo, and M. Yao, Dissociation mechanism from highly charged bromophenol: *Ab initio* molecular dynamics simulations, Z. Phys. Chem. **235**, 169 (2021).

[60] Z. Li, L. Inhester, C. Liekhus-Schmaltz, B. F. E. Curchod, J. W. Snyder, Jr., N. Medvedev, J. Cryan, T. Osipov, S. Pabst, O. Vendrell, P. Bucksbaum, and T. J. Martinez, Ultrafast isomerization in acetylene dication after carbon K-shell ionization, Nat. Commun. **8**, 453 (2017).

[61] C. E. Liekhus-Schmaltz, I. Tenney, T. Osipov, A. Sanchez-Gonzalez, N. Berrah, R. Boll, C. Bomme, C. Bostedt, J. D. Bozek, S. Carron, R. Coffee, J. Devin, B. Erk, K. R. Ferguson, R. W. Field, L. Foucar, L. J. Frasinski, J. M. Glownia, M. Gühr, A. Kamalov, *et al.*, Ultrafast isomerization initiated by X-ray core ionization, Nat. Commun. **6**, 8199 (2015).

[62] S. Maclot, D. G. Piekarski, A. Domaracka, A. Méry, V. Vizcaino, L. Adoui, F. Martín, M. Alcamí, B. A. Huber, P. Rousseau, and S. Díaz-Tendero, Dynamics of glycine dications in the gas phase: Ultrafast intramolecular hydrogen migration versus Coulomb repulsion, J. Phys. Chem. Lett. **4**, 3903 (2013).